Available online at www.sciencedirect.com
SCIENCE DIRECT®
Journal of Physics and Chemistry of Solids 66 (2005) 2163–2167
JOURNAL OF PHYSICS AND CHEMISTRY OF SOLIDS
www.elsevier.com/locate/jpcs

Resonant inelastic X-ray scattering (RIXS) spectroscopy at the Mn K absorption pre-edge—a direct probe of the 3d orbitals

Pieter Glatzel [a,*], Junko Yano [b], Uwe Bergmann [c], Hendrik Visser [b], John H. Robblee [b], Weiwei Gu [d], Frank M.F. de Groot [e], Stephen P. Cramer [d], Vittal K. Yachandra [b]

[a] European Synchrotron Radiation Facility, BP 220, F-38043 Grenoble Cedex, France
[b] Physical Biosciences Division, Melvin Calvin Laboratory, Lawrence Berkeley National Laboratory, Berkeley, CA 94720, USA
[c] The Stanford Synchrotron Radiation Laboratory, 2575 Sand Hill Road, Menlo Park, CA 94025, USA
[d] Department of Applied Science, University of California, Davis, CA 95616, USA
[e] Department of Inorganic Chemistry and Catalysis, Utrecht University, 3584 CA Utrecht, The Netherlands

Abstract

A study of the Mn K absorption pre-edges in oxides using resonant inelastic X-ray scattering (RIXS) spectroscopy is presented. The energy transfer dimension enhances the separation of the pre-edge (predominantly 1s to 3d transitions) from the main K-edge and a detailed analysis is thus possible. The RIXS spectra are sensitive to the Mn spin state. The technique thus yields detailed information on the electronic structure that is not accessible in conventional K-edge absorption spectroscopy. The line splittings can be understood within a ligand field multiplet model, showing the importance of (2p,3d) two-electron interactions that give rise to the spin-sensitivity.

Keywords: A inorganic compounds; C XAFS; D crystal fields; D electronic structure

1. Introduction

The X-ray absorption near edge structure (XANES) of the Mn K-edge absorption spectrum mainly reflects the Mn p-orbital contribution to the unoccupied orbitals due to the dipole selection rules. Mn XANES spectra have been used for example to monitor changes in the Mn oxidation state in biocatalysis [1]. Interpretation of XANES is difficult because of the many factors that influence the spectral shape [2]. A weak spectral feature arises at incident photon energies lower than the main K absorption edge (cf. Fig. 1). The potential of this K absorption pre-edge feature to extract information on the metal atom electronic structure and the local symmetry at the metal site is well known [3]. However, the K pre-edge spectral features are usually weak compared to the main edge because they mostly draw their intensities from quadrupole transition matrix elements. Furthermore, the energy separation between pre-edge and main edge decreases towards the early transition metals. A detailed analysis of the K pre-edge spectral features in conventional absorption spectroscopy is therefore often limited and associated with a rather large uncertainty because a strong background from dipole allowed transition at higher energies has to be subtracted. Hence, only few such studies are available for Mn [4].

The resonant inelastic X-ray scattering (RIXS) process is theoretically described by the Kramers–Heisenberg formula [5]:

$$F(\Omega,\omega)=\sum_f\left|\sum_i\frac{\langle f|T_2|n\rangle\langle n|T_1|g\rangle}{E_g-E_i+\Omega-i\frac{\Gamma_K}{2}}\right|^2\frac{\frac{\Gamma_L}{2\pi}}{(E_g-E_f+\Omega-\omega)^2+\frac{\Gamma_L^2}{4}} \quad (1)$$

The intermediate state $|n\rangle$ is reached from the ground state $|g\rangle$ via a transition operator T_1. In a simplified picture using atomic configuration we can write $|g\rangle=3d^n$ and $|n\rangle=1s3d^{n+1}$, i.e. a 1s electron is resonantly excited into a 3d orbital. The intermediate states $|n\rangle$ in 1s2p RIXS spectroscopy are the final states in conventional K-edge absorption spectroscopy. T_1 identifies with the quadrupole transition operator if the scattering atom is six-coordinated with identical ligands in an octahedral geometry (O_h symmetry). The K pre-edge can obtain some contribution from dipole transitions if the local symmetry is lower than O_h.

* Corresponding author
E-mail addresses: pieter.glatzel@gmx.org (P. Glatzel), bergmann@slac.stanford.edu (U. Bergmann), cramer@batnet.com (S.P. Cramer), vkyachandra@lbl.gov (V.K. Yachandra).

0022-3697/$ - see front matter © 2005 Elsevier Ltd. All rights reserved.
doi:10.1016/j.jpcs.2005.09.012

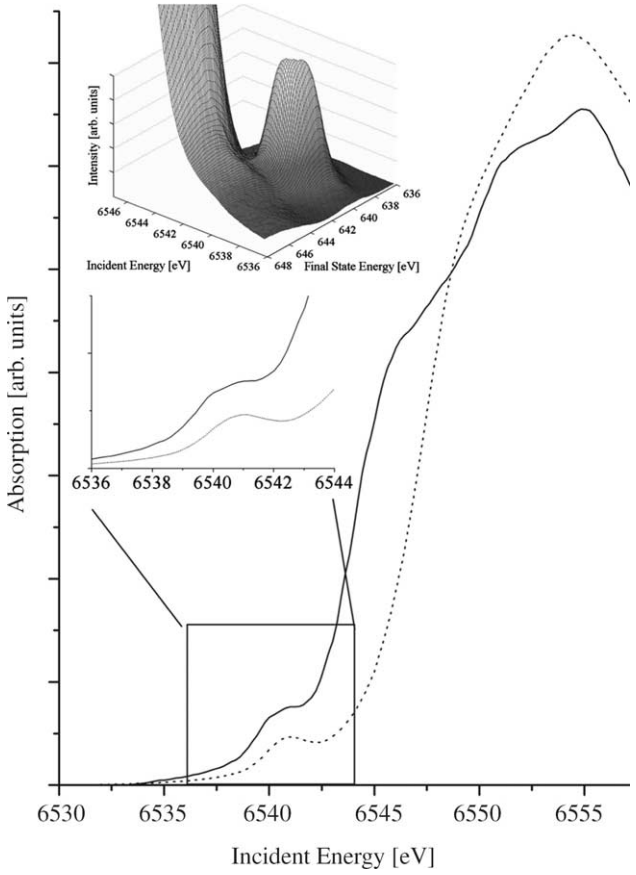

Fig. 1. Mn K-edge XANES in MnO (solid) and $Mn(acac)_2(H_2O)_2$. The lower inset shows the pre-edge region. The upper inset shows the 1s2p (L_3) RIXS surface plot at the pre-edge of MnO.

The final states are reached via a 2p to 1s transition and T_2, therefore, identifies with the dipole operator. The 1s2p RIXS final state configuration $|f\rangle = 2p^5 3d^{n+1}$ is identical to the final state configuration in soft X-ray L-edge absorption spectroscopy. Transition metal L-edge spectra with their pronounced chemical sensitivity have been discussed in depth by numerous authors [6,7]. In particular, it was found that the strong (2p,3d) multiplet interaction makes the L-edge more sensitive to the metal spin state. The same interaction also occurs in the 1s2p RIXS final states. In a RIXS study of a series of Ni coordination complexes similar spectral shapes as in L-edge spectroscopy were found in the energy transfer direction of the RIXS data thus demonstrating that RIXS is also sensitive to the metal spin state [8].

The incident energy Ω as well as the emitted energy ω are varied in a RIXS experiment. The recorded intensity is proportional to $F(\Omega,\omega)$ (cf. Eq. (1)) and is thus plotted versus a two-dimensional grid. In order to assign the total energy of an electronic state to the axes of the spectra we will use the energy transfer or final state energy $\Omega-\omega$ The energy transfer axis relates to the excitation energy in L-edge absorption spectroscopy.

2. Materials and methods

2.1. Mn model complexes

MnO, $Mn(acac)_2(H_2O)_2$, Mn_3O_4, Mn_2O_3 and MnO_2 were purchased from Alpha products. In order to minimize fluorescence 'saturation' and transmission 'leakage' artifacts, the samples were made optically thin by diluting the pure sample with boron nitride [9]. In all systems, Mn is six-coordinated with oxygen ligands and the local symmetry can be approximated by octahedral (O_h).

2.2. Synchrotron beamline

The RIXS data were recorded on the BioCAT undulator beamline 18-ID at the Advanced Photon Source [10]. The energy of the incoming synchrotron beam was selected by means of a nitrogen-cooled Si double-crystal monochromator with a (1,1,1) orientation. The sample was oriented at 45° relative to the incident beam and the beam size on the sample was 2.8 mm horizontal and 0.2 mm vertical FWHM. Higher harmonics were rejected by the focusing mirror. Using the fundamental undulator peak, the maximum incident flux was $\sim 10^{13}$ photons/s at 6.5 keV. The incident X-ray monochromator energy bandwidth (FWHM) is approximately 1.0 eV at 6540 eV. The monochromator energy calibration was constantly checked by recording the K pre-edge peak of $KMnO_4$ using two additional ion-chambers downstream of the sample.

2.3. Spectroscopy measurements

The scattered X-rays were collected by means of a crystal array spectrometer [11]. The (3,3,3) Bragg reflection of four spherically bent Ge crystals arranged in Rowland geometry was used. The analyzer crystals captured a solid angle of 3.4×10^{-2} sr. A nitrogen-cooled solid state (Ge) detector was placed at the common focus of the four crystals and the entire emitted beam path was enclosed by a He-filled bag. We determined an intrinsic analyzer bandwidth of 0.8 eV by measuring the elastically scattered peak and assuming a 1.0 eV primary monochromator energy bandwidth. The spectrometer was calibrated by measuring the absolute angle of the Bragg reflection using optical tools. We estimate that the upper limit for the error of the absolute analyzer energy calibration is 1 eV.

All samples were kept in a liquid He cooled cryostat below 10 K and surrounded by an exchange gas (He). Systematic radiation damage studies were performed for all compounds. The beam position on the sample could be adjusted vertically and horizontally and the total illumination time per sample position was kept below the time limit when damage occurred. To obtain the two-dimensional RIXS plane we recorded constant emission energy ω (CEE) scans ('on-the-fly' data acquisition) with the spectrometer energy changed stepwise. Each scan corresponds to a diagonal cut in the $(\Omega,\Omega-\omega)$ plane. The experimental RIXS plane was splined on an energy grid with equal energy steps of 0.1 eV in both directions. A constant

background was subtracted from all RIXS spectra. Intensity due to excitations at incident energies higher than the pre-edge was subtracted from the RIXS spectra similar to main edge subtraction in conventional absorption spectroscopy [12].

3. Results and discussion

The 1s2p (L_3) RIXS surface plot at the Mn K absorption pre-edge of MnO is shown in Fig. 1. Comparison with the conventional absorption spectrum shows how the pre-edge structure is better separated from the main edge in the RIXS spectrum. Subtraction of the main edge is now possible with less ambiguity than in conventional absorption spectroscopy.

The 1s2p (L_3) RIXS spectra of the three Mn oxides and $Mn(acac)_2(H_2O)_2$ are shown in Fig. 2. The MnO pre-edge structure stretches diagonally over about 2 eV indicating that at least two strong resonances form the spectrum. We will show below that the pre-edge for Mn^{2+} is solely split by the crystal field. MnO and Mn_2O_3 show pre-edge intensity at around 6540.5 eV. However, for Mn_2O_3 the peak appears sharper and symmetric compared to MnO even though the crystal field splitting is larger. Multiplet interactions (i.e. (3d,3d) Slater integrals) are important for a Mn^{3+} ion that result in line splittings on the order of the crystal field [12].

There is additional spectral intensity for Mn_2O_3 at $\sim$6543.5 eV incident energy. The spectrum is different for MnO_2 where only one broad structure is visible with one maximum and pronounced tails towards higher and lower energies. All experimental spectra, in particular the Mn(II) systems MnO and $Mn(acac)_2(H_2O)_2$, show asymmetric line shapes with shoulders in the direction of the energy transfer. These features are caused by electron-electron interactions that occur in the $2p^5 3d^{n+1}$ final states but not in the $1s3d^{n+1}$ intermediate states.

The K absorption pre-edges show a strong dependence on the Mn oxidation state. The center of gravity of the entire pre-edge structure moves to higher energies with increasing oxidation state. Unlike the XANES spectral shape they are less dependent on interatomic distances. The two Mn(II) systems nicely demonstrate that the pre-edge is more useful as a diagnostic to determine oxidation states than the main edge. While a strong shift between MnO and $Mn_2(acac)_2(H_2O)_2$ is observed in the XANES (Fig. 1) the two systems give equal center-of-gravity values for the K pre-edge [12]. The smaller crystal field splitting in $Mn_2(acac)_2(H_2O)_2$ gives a sharper peak.

In order to simulate the K pre-edge spectral shape we use multiplet theory that is based on atomic wave function calculations but includes a crystal field [13]. In this first, qualitative understanding of the Mn K pre-edges we consider the ionic cases of Mn^{2+} in octahedral (O_h) environment.

The 1s to 3d quadrupole and 2p to 1s dipole transition matrix elements were calculated and fed into the Kramers-

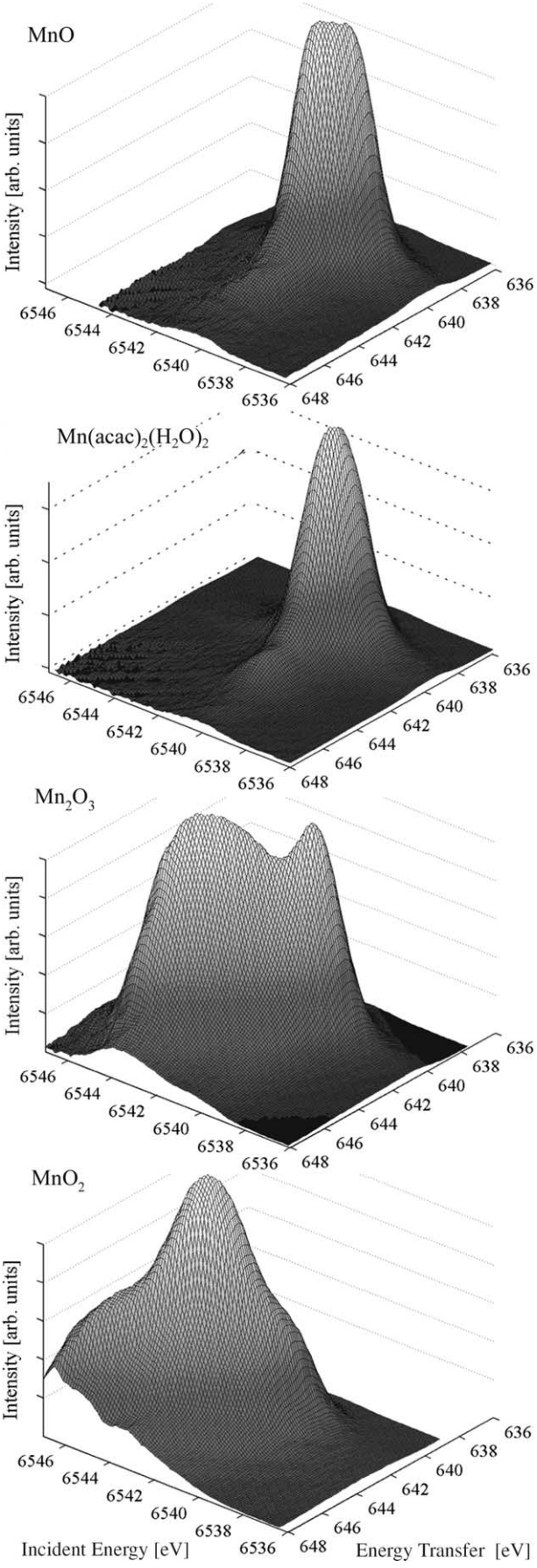

Fig. 2. 1s2p RIXS surface plots for the Mn oxides and $Mn(acac)_2(H_2O)_2$; The main edge is subtracted and only the K pre-edge resonances in the L_3 final states are shown.

Heisenberg equation to yield the 1s2p RIXS spectrum. A ligand field splitting of 10 Dq = 1.1 eV was assumed and the Slater integrals were scaled down to 80% of their atomic values. The crystal field splitting was obtained by fitting the experimental spectrum. We used a 1.1 eV (0.5 eV) Lorentzian and a 1.0 eV (0.8 eV) Gaussian line shape to account for lifetime and instrumental broadening in the intermediate (final) state, respectively. The absolute configuration energies in Hartree-Fock self consistent field calculations are not accurate [14]. The calculated spectra were therefore shifted in energy to correspond with the experimental spectrum. Using the same parameters, we also calculated the absorption L-edge.

The calculated Mn^{2+} spectrum in Fig. 3 reproduces the spectral shape in MnO very well. The two strong resonances are separated by the crystal field splitting 10 Dq. They are not resolved in the convoluted spectrum due to the 1s core hole lifetime broadening. The slight differences in intensity between theory and experiment are due to orbital hybridization that is not included in the calculations. The weak shoulder in the final state energy direction, that only becomes visible after subtraction of the main edge, is reproduced in the calculations. It arises from multiplet interactions in the $2p^5 3d^6$ final state configuration.

Crystal field multiplet calculations for a Mn^{2+} ion in octahedral symmetry thus accurately reproduce the MnO 1s2p RIXS spectral shape, which shows that MnO forms an essentially pure $3d^5\ ^6A_1$ ground state. The ground state sextet spin multiplicity has a strong stabilizing effect on the electronic structure because of the (3d,3d) 'exchange' interaction between electrons with parallel spins. This is confirmed experimentally by the equal center-of-gravity position of the pre-edge in MnO and $Mn(acac)_2(H_2O)_2$. All electron-electron multiplet splittings are absent in the $1s3d^6$ excited state of Mn^{2+} because of the $^6A_1$ ground state symmetry. The final state (2p,3d) multiplet interactions are present and sensitive to the metal atom spin state. The weak shoulder along the energy transfer is indicative for a Mn^{2+} high-spin configuration as has been shown in soft X-ray L-edge spectroscopy [7].

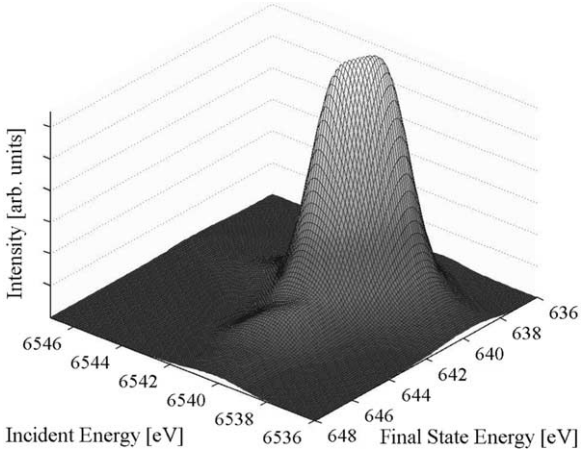

Fig. 3. Calculated 1s2p (L_3) RIXS surface plot based on ligand field multiplet calculations for a Mn^{2+} ion in octahedral symmetry with 10 Dq = 1.1 eV.

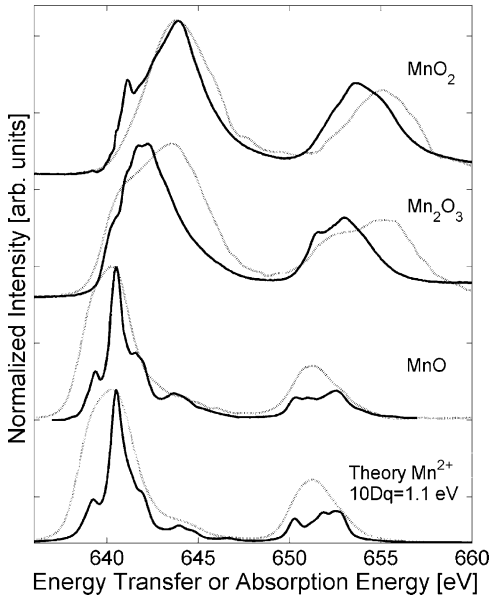

Fig. 4. 1s2p RIXS energy transfer spectra for the Mn oxides (dashed) compared to L-edge absorption (solid) and crystal field multiplet calculations.

We compare in Fig. 4 the energy transfer spectra for the Mn oxides to the L-edge absorption spectra (taken from Ref. [15]). The energy transfer spectra were obtained by integrating the RIXS plane (after main edge subtraction) along the incident energy in the range of the pre-edge. The relative line intensities in the RIXS spectra are different from the L-edges while the shift to higher energies with increasing oxidation state can be observed in both techniques. Analysis of the $I(L_3)/I(L_3+L_2)$ branching ratio does not give a dependence on the oxidation state for 1s2p RIXS. The RIXS final states are reached via two transition matrix elements and we thus expect indeed that the relative line intensities differ between 1s2p RIXS and absorption L-edge. The calculations accurately reproduce the differences between the two techniques for MnO.

4. Summary and outlook

RIXS spectroscopy greatly facilitates analysis of the K absorption pre-edges in Mn systems. The technique is furthermore sensitive to the valence electron spin-state via the (2p,3d) interaction in the final state. The energy transfer spectral resolution is only limited by the 2p core-hole lifetime of 0.5 eV. With some technical effort, future instrumental energy broadening of <0.6 eV should be obtainable at a realistic efficiency. This will allow for a more detailed analysis of both intermediate and final state effects, and thus provide new information on the electronic structure of numerous chemically important 3d metal systems.

Acknowledgements

This work was supported by the National Institutes of Health (Grant GM55302 (V.K.Y), GM44380 and GM65440 (S.P.C)), National Science Foundation (Grant CHE-0213952 (S.P.C.)) and the Director, Office of Science, Office of Basic

Energy Sciences, Division of Chemical Sciences, Geosciences, and Biosciences, of the US Department of Energy (DOE), under Contract DE-AC03-76SF00098 (V.K.Y.) and DOE Office of Biological and Environmental Research (S.P.C.). The research of PG and FMFdG is supported by grants from Netherlands Scientific Organization-Chemical-Sciences (NWO-CW). UB was supported by the Stanford Synchrotron Radiation Laboratory, Department of Energy, Office of Basic Energy Sciences contract DE-AC03-765F00515. Use of the Advanced Photon Source was supported by the U.S. Department of Energy, Basic Energy Sciences, Office of Science, under contract No. W-31-109-ENG-38. BioCAT is a National Institutes of Health-supported Research Center RR-08630.

References

[1] J.E. Penner-Hahn, R.M. Fronko, V.L. Pecoraro, C.F. Yocum, S.D. Betts, N.R. Bowlby, J. Am. Chem. Soc. 112 (7) (1990) 2549–2557; V.K. Yachandra, K. Sauer, M.P. Klein, Chem. Rev. 96 (7) (1996) 2927–2950.

[2] J.J. Rehr, R.C. Albers, Rev. Mod. Phys. 72 (3) (2000) 621–654; A.H. de Vries, L. Hozoi, R. Broer, Int. J. Quant. Chem. 91 (1) (2003) 57–61.

[3] T.E. Westre, P. Kennepohl, J.G. DeWitt, B. Hedman, K.O. Hodgson, E.I. Solomon, J. Am. Chem. Soc. 119 (27) (1997) 6297–6314; M. Wilke, F. Farges, P.E. Petit, G.E. Brown, F. Martin, Am. Mineral. 86 (5/6) (2001) 714–730; P. Glatzel, U. Bergmann, Coord. Chem. Rev. 249 (1) (2005) 65–95.

[4] H. Visser, E. Anxolabehere-Mallart, U. Bergmann, P. Glatzel, J.H. Robblee, S.P. Cramer, J.J. Girerd, K. Sauer, M.P. Klein, V.K. Yachandra, J. Am. Chem. Soc. 123 (29) (2001) 7031–7039; H. Hayashi, M. Kawata, R. Takeda, Y. Udagawa, Y. Watanabe, T. Takano, S. Nanao, N. Kawamura, J. Electron Spectrosc. Relat. Phenom. 136 (1/2) (2004) 191–197; H. Shoji, M. Taguchi, E. Hirai, T. Iwazumi, A. Kotani, S. Nanao, Y. Isozumi, J. Phys. Soc. Jpn 72 (6) (2003) 1560–1569.

[5] A. Kotani, S. Shin, Rev. Mod. Phys. 73 (1) (2001) 203–246; F. Gel'mukhanov, H. Ågren, Phys. Rep.—Rev. Sec. Phys. Lett. 312 (3/6) (1999) 91–330.

[6] F.M.F. de Groot, J. Electron Spectrosc. Relat. Phenom. 676 (4) (1994) 529–622; B. Gilbert, B.H. Frazer, A. Belz, P.G. Conrad, K.H. Nealson, D. Haskel, J.C. Lang, G. Srajer, G. De Stasio, J. Phys. Chem. A 107 (2003) 2839–2847.

[7] S.P. Cramer, F.M.F. de Groot, Y. Ma, C.T. Chen, F. Sette, C.A. Kipke, D.M. Eichhorn, M.K. Chan, W.H. Armstrong, E. Libby, G. Christou, S. Brooker, V. Mckee, O.C. Mullins, J.C. Fuggle, J. Am. Chem. Soc. 113 (21) (1991) 7937–7940.

[8] P. Glatzel, U. Bergmann, W.W. Gu, H.X. Wang, S. Stepanov, B.S. Mandimutsira, C.G. Riordan, C.P. Horwitz, T. Collins, S.P. Cramer, J. Am. Chem. Soc. 124 (33) (2002) 9668–9669.

[9] J. Goulon, C. Goulon-Ginet, R. Cortes, J.M. Dubois, J. Physiol.—Paris 43 (1982) 539–548.

[10] G.B. Bunker, T. Irving, E. Black, K. Zhang, R. Fischetti, S. Wang, S. Stepanov, BioCAT Undulator Beamline at APS, Ithaca, 1997, p. 16.

[11] In A high-resolution large-acceptance analyzer for X-ray fluorescence and raman spectroscopy, in: U. Bergmann, S.P. Cramer (Eds.), Crystal and Multilayer Optics, San Diego, SPIE, San Diego, 1998, pp. 198–209.

[12] P. Glatzel, U. Bergmann, J. Yano, H. Visser, J. Robblee, W. Gu, F.M.F.D. Groot, V.L. Pecoraro, G. Christou, S.P. Cramer, V.K. Yachandra, J. Am. Chem. Soc. 126 (32) (2004) 9946–9959.

[13] J.C. Slater, Quantum Theory of Atomic Structure, McGraw-Hill, New York, 1960; T. Thole, R.D. Cowan, G.A. Sawatzky, J. Fink, J.C. Fuggle, Phys. Rev. B, 316856.

[14] A. Meisel, G. Leonhardt, R. Szargan, X-Ray Spectra and Chemical Binding, Springer, New York, 1989.

[15] F. Morales, F.M.F. de Groot, P. Glatzel, E. Kleimenov, H. Bluhm, M. Havecker, A. Knop-Gericke, B.M. Weckhuysen, J. Phys. Chem. B 108 (41) (2004) 16201–16207.